48th AIAA Aerospace Sciences Meeting Including the New Horizons Forum and Aerospace Exposition
4 - 7 January 2010, Orlando, Florida

AIAA 2010-1603

Aspects of Numerical Analysis for Unsteady Flows in Aircraft Engines

Jixian Yao*
GE Global Research, Niskayuna, NY 12309

Patricia L. Cargill†
GE Aviation, Cincinnati, OH 45246

D. Graham Holmes‡
GE Global Research, Niskayuna, NY 12309

and

Steven E. Gorrell§
Brigham Young University, Provo, UT 84602

This paper reviews a few select topics of high-fidelity numerical simulations for unsteady flows in the turbomachinery components of aircraft engines. Topics include the high-performance computing and flow solver, role of unsteady flow analysis in engine design and development, interrogation and interpretation of the unsteady flow physics. A cost-effective low-speed preconditioning formulation is discussed. A faster alternative algorithm to dual-time stepping scheme is provided. Loss auditing techniques and deterministic stress modeling are discussed as well. Highlights of numerical analysis for inlet distortion transfer and generation in the engine compression components are presented. A brief elaboration of challenges and outlook of high-fidelity numerical analysis is also included in the paper.

Nomenclature

c	=	speed of sound
C_p	=	specific heat at constant pressure
f	=	time ratio of serial portion of a parallel CFD code
g	=	overhead cost in real-world parallel applications
H, h, h_0	=	total enthalpy
N	=	number of processes in a parallel application
p, p_0	=	pressure (static and stagnation)
P_0, P_c	=	low-speed preconditioning matrix
q, q_i	=	total velocity, heat flux
S, s	=	speed-up factor of a parallel flow solver, specific entropy
T, t	=	temperature, time
u,v,w	=	Cartesian velocity components

I. Introduction

Great advances in efficiency and power density have been made in turbomachines over the past century and a half. This progress has, in large part, been the result of greater understanding of the complex physics of these conceptually simple machines. The understanding has come from experimental, analytical, and more recently

* GE Global Research, One Research Circle, Niskayuna, NY 12309 USA. yaoj@ge.com
† GE Aviation, Fan/Compressor Aero Design, Cincinnati, OH 45246, USA.
‡ GE Global Research, One Research Circle, Niskayuna, NY 12309, USA.
§ Brigham Young University, Provo, UT 84602, USA.

numerical techniques. Today, numerical methods (Computational Fluid Dynamics or CFD) are a key tool for the design of turbomachines. Until recently, most of the numerical analysis of turbomachinery flow has been based on two key simplifying assumptions. The first is that the flow in each blade row is steady in the reference frame of that blade row; the second is that the flows in every blade passage in a row are identical. It is remarkable – and little remarked upon – that these two gross simplifications have been so successful in facilitating useful predictions of performance, and in affording a rich understanding of the flow physics.

Ever greater demands for energy efficiency, in both aviation industry and power generation field, require that these two assumptions be revisited. There is growing consensus that the next significant increase of efficiency will only be realized via an understanding of unsteady flow physics in turbomachines. Unlike steady-state flows, unsteady flows have unique aspects in behavior and aerodynamic properties. Whenever the static pressure is time unsteady, the total enthalpy varies accordingly. This, in turn, could generate commensurate changes in total pressure without even affecting the aerodynamic loss. Unsteady flows in aircraft engines often involve a large range of length and time scales. Length scales vary from tip clearance gaps to the diameter of the component; time scales vary from the period of trailing edge vortex shedding to blade passing periods, and to wheel rotation. The paper will illustrate these aspects of unsteady flows via several examples. Unsteady flow interrogation and interpretation techniques and loss-auditing approaches will also be discussed.

Compared to the steady-state flow analysis, the unsteady flow simulation requires much greater compute resources and is time-consuming. There are various numerical techniques that help mitigate the computational cost of adding the extra dimension of time, i.e. linearization or phase-lag assumptions. But a truly general-purpose analysis of unsteady flows requires a massive increase in computational effort. This is because the relaxation of the assumption of steady-state flows necessitates the relaxation of the assumption that all blade passages in a row are alike. The following examples illustrate the unsteady nature of the flows: (1) A transonic fan fluttering with the phase of the blade motion varying around the annulus; (2) The unsteady interaction between a rotor and a stator while ingesting a low engine-order inlet flow distortion; and (3) The pressure perturbation due to fan rotation and blade vibration interacting with acoustic modes of an engine inlet. In the following sections, we will discuss the unique challenges of high performance computing, including the parallelization of flow solvers for high parallel efficiency and scalability on today's massively parallel computers, and strategies and techniques for achieving robust and quick turn-around for unsteady flow calculations.

Numerical analyses for unsteady flow were applied to aircraft engines and, in general, turbomachinery since the early 90's of the last century. Thanks to the advances in both computer technology and numerical algorithms, unsteady flow simulations have made great progress, growing from blade row interactions to component interactions. Unsteady flow analysis, regardless of its domain size, must serve as an effective tool for aircraft engine design. A great deal of unsteady flow physics has been understood via numerical simulations in the past. New physics is still being discovered and learned today. We must go one step further to bridge the unsteady flow analysis and engine design, and to incorporate what we have learned to new engine design in a tangible and definitive way.

This paper is organized in the following manner. The role of unsteady CFD in engine design is discussed first and foremost in Section II. Section III is focused on the requirement and techniques of high-fidelity numerical simulations, which includes planning and jugular experiments, parallel efficiency and scalability of flow solvers, a cost-effective low-speed preconditioning algorithm, and an alternative numerical algorithm for unsteady flows. In Section IV, examples of large-scale unsteady flow simulations are provided to highlight some aspects of unsteady flow physics we have learned. Examples include HPT/LPT interactions, inlet distortion generation and transfer in multi-stage fans, and nacelle/fan/OGV interaction in a commercial engine. In the final sections, an elaboration of challenges and outlook of Hi-Fi numerical simulation is made, and a brief conclusion is added.

II. Role of Unsteady CFD in Engine Design and Development

This section seeks to address how unsteady flow simulations should be used as a design tool, and how it can affect engine designs.

In some cases, unsteady flow analyses are now well integrated into the regular design process for turbomachinery. Aeromechanics applications, including prediction of airfoil flutter with a single-airfoil analysis as well as prediction of airfoil vibratory response to upstream wake excitation with two-airfoil analysis, are routinely executed during airfoil designs. Although they can be inconveniently time-consuming, and their accuracy is not perfect, they are vastly superior to previous methods, and so have been incorporated into the design process.

In contrast, the large-scale analyses of multiple blade rows discussed later in this paper are currently too unwieldy to be fully integrated into everyday design iterations. Logistical challenges form one barrier: the sheer size of the cases can make them difficult to set up, run to convergence, and post-process; and often taxes the

available computation hardware and software to their limits. The other area of challenge is uncertainty in how to interpret and make use of the results, perhaps due to limited validation but also due to inexperience in post-processing, averaging, and visualizing such solutions. However, these large-scale analyses on special cases are proving helpful by leading the design community to new insights into the flow physics.

Although flow fields in turbomachinery are extremely complex, especially as higher-order effects are included in the modeling, the task of the designer is to constantly push his understanding to new levels. Even before a new model is developed to the point of accurately predicting all quantitative properties, the qualitative results can guide the thinking of the designer into new areas. This can then give rise to new ideas of how to change a design to modify the flow for the better, although these ideas must then be tried and validated, often by physical testing. For example, the non-axisymetric and unsteady flow field around a fan OGV produces variations in incidence on the OGV. Once these variations are quantified, the designer can account for them in his design without needing to run the complex analysis on every design iteration. In another case, if he can gain insight into how a multi-stage fan responds to inlet distortion from one large analysis, the astute designer can alter his design strategy appropriately, again without needing to run the large analysis on every design iteration.

Another benefit of these high fidelity analyses is that they can help the designer better understand and interpret test data. For example, it is impossible to instrument a fan in flight test to completely characterize the flow field with all its spatial and temporal variations. Large-scale analyses, when well grounded in existing data, can help "fill in the blanks" between measurements and help in understanding larger trends.

New insights can also aid in the development of lower order (simpler) models that are more amenable to application to everyday design iterations. In the area of compressor stability and the effects of inlet distortion, large-scale unsteady analyses are guiding improvements in the fidelity of one-dimensional stability models. Coupled analysis of a fan and inlet can spur ideas for different boundary conditions that may allow de-coupled analyses with higher accuracy. It is hoped that careful investigations of unsteady analyses of multiple blade rows will help enable further development of closure models for steady multi-stage models to the point where they can be confidently used for state-of-the art designs.

For these benefits to materialize, it is essential that the designer understand the current state of an analytical model and use it appropriately, avoiding the dual pitfalls of, on one hand, under-utilizing a tool that could be very helpful and, conversely, relying excessively on a tool without regard for its limitations. The ability to hit this "sweet spot" of appropriate utilization of models in turbomachinery design is a key factor in aggressively advancing the state of the art while avoiding missteps that can prove extremely costly in the aviation industry. Very close collaboration and knowledge sharing between the design community and the model development community is critical to this process, all the way from initial development of the model and its processes, through special applications, to the ultimate goal of a well-developed, highly accurate, simple-to-use tool that can be applied with confidence.

Ultimately, of course, it is assumed and eagerly anticipated that advances in computer hardware and unsteady modeling will continue apace, to the point where large-scale multi-stage full-annulus analyses are regularly performed on design iterations and relied upon for quantitative comparison of design alternatives.

III. Requirement for High-Fidelity Numerical Simulations

This section outlines four aspects of high-fidelity numerical simulations. These aspects highlight the challenges of improving parallel efficiency and scalability of CFD flow solvers that employ structured grid and use coarse-grain domain-decomposition for parallel applications. Techniques and algorithms are presented in this section as well aiming to reduce the time-to-solution for unsteady flows.

A. Planning of Hi-Fi Simulations

It's easy to state that Hi-Fi numerical simulations require a vast amount of computing resources and fast, accurate and robust CFD solvers. While this is true, however, the first and foremost requirement is to have a crystal clear vision. Hi-Fi numerical simulations need to be purpose-driven. We need to determine whether the Hi-Fi CFD is the appropriate strategy to achieve the objective. We should not perform them just because we can, or as a "stunt" calculation without a purpose. Parallel computing is not a brute-force method to overcome limitations of the baseline algorithms/solution procedures. It is not a "cool" way of getting solutions faster; it is certainly not an absolute need for every existing application.

At the stage of planning, we need to consider not only numerical analysis, but also theoretical analysis, experimental evidence, and fluid dynamics experience. Combining the three is most useful[1,2,3]. The outcome of this planning is to make clear the appropriate flow regime involved, the proper domain that needs to be built with well-

posed boundary conditions that make engineering sense and are easy to provide, and the fluid dynamic disciplines and range of length and time scales that might be involved. Each of the simulations should be tailored to deliver something that serves the overall objective, be it an engineering finding, a loss mechanism, an exploration, or a numerical experiment. Past CFD experiences could be drawn on for this planning. If design modifications are involved, they will have to be considered as well. Possible outcomes can also be debated and risk abatement discussed at this stage.

High-fidelity unsteady simulations may require tens of thousands or hundreds of thousands - or even millions - of CPU hours to complete. A compute resource on this scale is not cheap. This places an interesting burden of those who develop and run CFD analyses. Typically, CFD runs are launched without meticulous preparation. If a case fails to run, or if it emerges that the solution did not produce the desired results, then the job input data can quickly be modified and the job resubmitted. This iterative approach has historically been justified because it is fast and inexpensive. For very large-scale simulations, this casual approach is no longer acceptable. CFD analysts have to begin to think like experimentalists: this "experiment" is going to cost this many thousands of dollars, and I have a scheduled opportunity to conduct the "experiment" in a particular window of time on a particular compute resource – so I had better make 100% sure that this one, expensive opportunity is not wasted.

B. Jugular Experiment

Some critical trial and error might need to take place especially when planning Hi-Fi CFD with too many uncertainties. One unique challenge in planning a Hi-Fi CFD is to determine the fidelity level that is appropriate to the engineering problem. This often ties in with the flow regime and length and time scales of the problem to solve. In a scenario that secondary small-scale flow structures could become a primary disturbance under unique circumstances, missing the smaller scale structures could affect the outcome of the entire simulation. A jugular experiment is then a critical step to address these issues. The experiment in and of itself needs careful planning as well to deliver answers to specific questions. It can also be a critical step for validation and verification of CFD solvers to be used in the simulations.

Take for example the simulation of circumferential distortion transfer in an axial flow fan system[4,5]. The flow regime is relatively simple. It mainly involves fluid dynamics, no intensive heat transfer. From a length/time scale perspective, the circumferential distortion is a long wavelength disturbance, while the blade row interaction is at least an order of magnitude smaller. There is also a potential of wake shedding that often have another magnitude smaller than blade row interaction. On top of this, we need to consider the resolution of hub/tip vortices. Industrial practices of grid resolution in hub/tip gaps range from 4 cells in the gap to 48 or more cells with carefully crafted meshing topology. We carried out a series of numerical trials to address the fidelity level issue with resolution of various flow features. For a simulation of a single blade passage with steady-state flow, we probably can get away with concentrating grid points near the solid walls, but for unsteady simulations, especially in a multi-blade-row environment, good grid resolution also needs to be considered within the passages away from boundary layers and in the axial gaps in between adjacent blade rows. This is necessary to capture and sustain wake migration and shockwave movement and hub/tip leakage flows and vortices. Grid resolution in the radial direction is also a concern so the blade (especially rotors) geometry is faithful to the real hardware and operating conditions[6]. Some of these concerns can be addressed from past blade row CFD experiences, but the limitations and preconditions need to be clearly borne in mind when taking experiences, as experiences always exist in a context. Another element we considered was the impact of "cold" or "hot" geometry, and the non-uniformity of the hub/tip clearances in the axial and in the circumferential directions.

For the simulations of distortion transfer in multistage axial fans, we had to carry out numerical trials on two selected smaller domains. One is a front stage of a fan, and the other is a rear stage of another fan that was designed differently. From experimental evidence and theoretical analysis, we knew that even if a fan is subject to only a pressure distortion at inlet, as a result of rotor response, it gives rise to total temperature distortion and swirl distortion in addition to the existing pressure distortion at rotor discharge. This flow condition is then ingested by the downstream stages. The first experiment with the front stage addresses the distortion generation issues, and the second experiment with the rear stage addresses multiple distortion transfer issues. Both address fan response issues to various flow conditions. To a large extent, the success of the two smaller experiments ultimately guarantees the success of the full scale simulations carried out on the two multistage fans.

C. Parallel Efficiency and Scalability of Flow Solvers

The performance evolution of microchips is put in historical perspective as shown on the left in Figure 1, adopted from Ref. 7. Up until year 2000, the processors simply became faster each year. After that, the chip clock speed is fixed or decreasing due to power consumption limitations. As a result, multi-core processors have become

the main processing units. Number of transistors would still double every 18 month only if the number of processors is increased. Parallelism is inevitable both to save energy and for reasonable price/performance ratio at the CPU level.

On the other hand, the landscape of parallel computer systems has evolved quite significantly, largely due to DoE's ASCI project started in 1997. Expensive and massive vector machines are gone, and inexpensive rack-mounted Linux cluster and super-clusters are becoming more commonplace. The performance of parallel computing systems has risen rapidly in the last decade, and the aerospace industry's use of high-performance computing has been on top and increasing steadily. However, we should not solely rely on the advances of the HPC systems for the growth of numerical simulation ability. The moral should be that both the computer systems and the numerical algorithms should be advanced. Compute power has increased more than 1000 times in the last decade. The speed of the numerical schemes has also increased close to 1000 times since the inception of CFD, such as local time stepping for steady-state flows, implicit schemes, and various convergence acceleration techniques such as multi-grid, residual smoothing, pre-conditioning. The fidelity of the numerical schemes has increased as well thanks to shock-capturing schemes and high-resolution schemes.

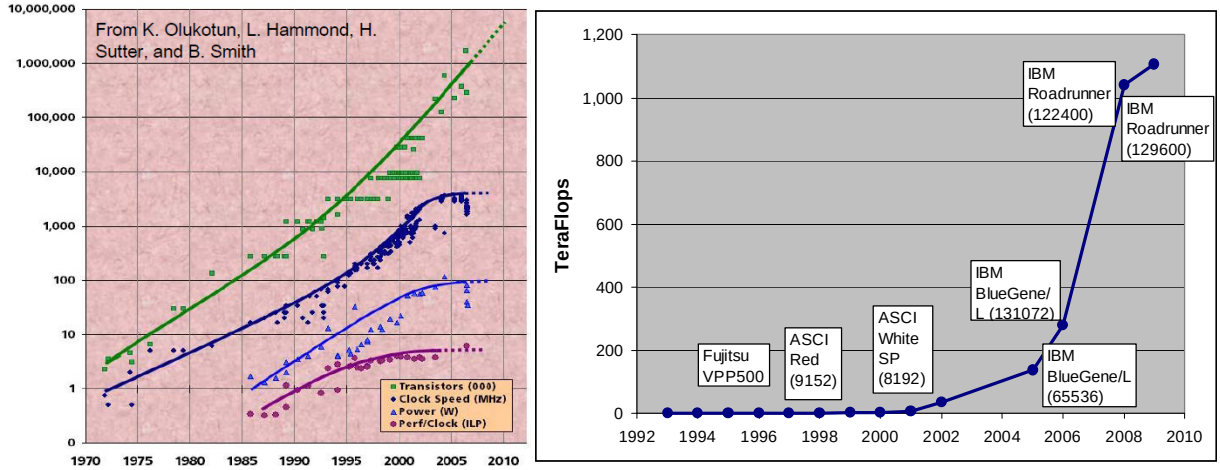

Figure 1. Performance evolution of microchips (left) and parallel computers (right)

The general objective of parallel computing is of course fast execution speed, which is achieved by enabling multiple analyses in a fixed amount of time, or by decreasing time necessary to complete one solution. Faster computers also allow us to increase modeling fidelity of our physical systems by either increasing grid resolution than possible in single processor machines or introducing additional physical models. For industrial research and development, cost and benefit of high-performance computing are important factors. Cost of parallel computers is always higher than collection of single units due to additional inter-connection and other expenses. The benefit, however, is usually derived from the product development that CFD serves to reduce development time, to produce higher performance, or to provide an opportunity to reduce the number of physical experiments and prototypes for a new engine. For this reason, we must consider the parallel efficiency and scalability of the flow solvers.

Parallel efficiency can be measured in two different ways. They are strong scaling and weak scaling. The strong scaling is based on Amdahl's law in which the problem size is fixed while the number of processors used to solve the problem is increased. Amdahl's law may not represent all the possible scenarios for real-world parallel applications, but it provides a simple yet powerful tool for us to gauge the parallel performance. For a given parallel code that consists of a serial portion (Ts) and a parallel portion (Tp), the speed-up factor is defined as the ratio of time on a single processor and the time on N processors. Define f=Ts/T, the speed-up factor takes the following form:

$$S = \frac{T(1)}{T(N)} = \frac{Ts + Tp}{Ts + \frac{Tp}{N}} = \frac{N}{1 + (N-1)f}$$

If we take into account for the real-world scenario, we need to add at least overhead time such as inter-processor communication in job control and data transfer, I/O tie-up, load overhead, and idle time due to load imbalance. This overhead is scalable to N: Toh=g*Tp*N, where g is a coefficient of the overhead time. The speed-up factor then becomes

$$S = \frac{N}{1 + (N-1)f + (1-f)gN^2} \quad .$$

If a code is 100% parallelizable, then f=0, the speed-up is ideal. Figure 2 is a plot of speed-up with various f. This simple plot reveals that if a code is 99% parallelizable (f=0.01), it can effectively scale to 100 processors. It has to be 99.9% parallelizable (f=0.001) to be effective with 1000 processors. In real world applications, especially in turbomachinery CFD applications, even 99% parallelization is quite difficult to achieve. The underlying assumption here is perfect load balance among all the processors. In addition to what we discussed above, the parallel overhead often increases when the fixed-size problem is decomposed into smaller and smaller "blocks" when increasing number of processors for the problem. Take for example a two-dimensional 100x100 grid with a cell-centered flow solver that uses "halo" cells to communicate and for boundary conditions. For a single processor application, there are 400 halo cells (assuming only one layer of halo cells), the overhead is 4%. When we equally divide the grid into 4 blocks, each block has 50x50 cells. The total halo cells are 800, overhead then becomes 8%. When we use 100 processors (100 blocks), the overhead reaches 40%! The speed-up actually deteriorates quickly as N increases. The scenario is depicted in Figure 2 when different overhead factor, g, is applied.

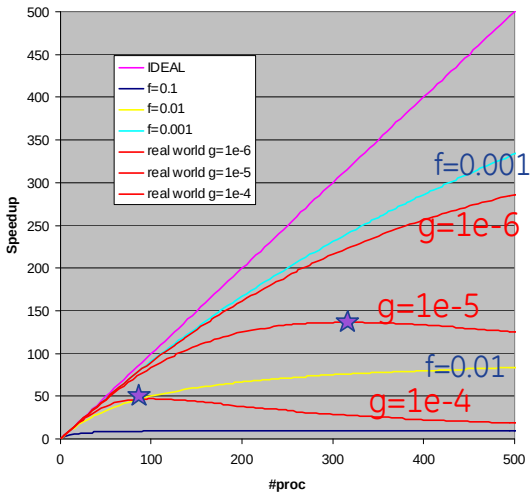

Figure 2. Parallel speed-up at various scenarios

However, this does not mean that we can only effectively use a few hundred processors. By increasing the problem size, the communication overhead can be kept at a low level. This leads to the weak scaling concept. Weak scaling is to maintain the same amount of time to solve a problem with increasing size by increasing the number of processors. Weak scaling hides the strong-scaling parallel efficiency, and is relatively easier to achieve. Weak scaling actually measures the scalability of parallel codes, rather then their efficiency. This does not translate, however, that we can get away with less-efficient parallel flow solvers. We should strive to make every possible means to improve the strong scaling efficiency to reduce the execution time for weak scaling applications. Techniques highlighted in Ref.8, though proposed and implemented in 2001, are still effective in turbomachinery code development today. These techniques ranged from 3D to 1D data structure inter-change, communication-weighted load balancing scheme, latency hiding, a single pass communication, and integrated boundary condition treatment to address all the communication needs. Single layer of halo cells on coarse grids in a multi-grid cycle, and the "data-pool" concept to deal with scalability for multi-blade row applications were developed and employed as well.

There are two major aspects that matter a great deal for real world applications with a flow solver that has fixed parallelism factor f. The first is load balancing. This goes into the detailed planning stage of parallel applications. A simple check at the ratio of maximum load and minimum load could be misleading; the distribution of the load needs to be considered as well. This is simply because the processor with largest load determines the overall parallel efficiency. A single processor with a load larger than the rest of the processors slows down everyone, but a processor with a lighter load than the rest has little effect in overall run time.

On the other hand, we should avoid decomposing the entire domain into tiny "blocks" just to get a near perfect load-balancing. The reason for this is discussed above. Communication overhead increases dramatically if the basic 'blocks' are too small which is defeating the purpose of load balancing. It is often limited for a perfect load balancing on a given set of structured multi-block grid. Therefore, the load-balancing actually needs to be considered in the grid generation phase of a parallel calculation. If multi-grid is used, one needs to consider splitable blocks with grid size that would be flexible.

The second aspect is I/O performance of the flow solver and the computer system (OS and hardware). The flow solver should not pose a roadblock due to I/O, and should use parallel I/O whenever possible. This is only one side of the problem though. Actually performance is determined by the file system architecture, how the OS handles

parallel I/O, and finally how the storage hardware performs on the read and write processes. I/O is often overlooked in large-scale calculation, but it can be a real threat to high parallel performance and scalability.

D. Visualization and Post-Processing

Managing and post-processing the data from large-scale unsteady analysis is not trivial. Time-accurate 3D simulations of this magnitude produce enormous amounts of data that may risk concealing rather than revealing the physics of interest. It is critical to know what the purpose of the analysis is and what results are desired from the simulation. For overall performance prediction, time-averaged values of efficiency, pressure ratio, and mass flow rate can be readily computed, but provide little insight into the flow field and will not contribute to the advancement of future designs. To analyze the unsteady flow physics, 3D animations and data mining are required to help determine where and how to look at the data. Scientific visualization is an integral part of performing such large-scale simulations. It is needed to analyze unsteady flow physics. Analysis is extremely time-consuming and the authors have realized that visualizing and post-processing large data sets require parallel tools.

The data management challenge is in finding useful information in terabytes of data without requiring massive memory storage and fast network bandwidth. Common flow features extracted are streamlines, vortices, shock waves, flow separation, and recirculation zones. The capability to do concurrent analysis, i.e., during the simulation run time, would ameliorate excessive post-processing storage needs by targeting specific regions where features have been detected. What is needed is an intelligent data mining capability that has both knowledge – descriptive physics of the situation and a cognitive model of what the human users need – and some foresight: some way to predict what the user might need to supplement the feature detection or not ignore unanticipated features that might be of interest. For instance, a researcher may be studying in detail turbulence in one region and find unexpected flow separation in an adjacent region.

A concept called Concurrent Agent-enabled Feature Extraction (CAFÉ)[9,10] is being developed to do concurrent feature extraction and data-mining in high-fidelity fluid dynamic simulations. Multiple agents running various data-mining algorithms at multiple nodes perform the process of feature extraction. Agents communicating in the information space share data in a collaborative environment. The individual agents utilizing evidential reasoning (based on a three-valued logic system that intrinsically accounts for data uncertainty) then calculate the likelihood that a feature exists, assist in visualizing the feature, and store the feature characteristics for later recall in other simulations. Machine learning provides the means for the feature learning such that CAFÉ is able to find the characteristics that are of particular interest to the researcher as quickly as possible.

CAFÉ is an extraction tool that can extract flow features concurrent with a running simulation and as a post-processing step that uses intelligent software agents to synthesize multiple feature extraction algorithm outputs into one final output containing only highly probable features. A rule base has been defined that governs intelligent software agents designed specifically to mine massive CFD data sets. The agent-based approach allows for the use of highly parallel extraction techniques, thereby maximizing the use of computing clusters. This capability will drastically reduce the data analysis time required for such complex systems.

E. Low-Speed Preconditioning for Dual-Time Stepping Algorithm

Most practical low-speed preconditioning is still based on inviscid characteristics of the governing equations. Turkel[11] introduced an effective preconditioning matrix, P_0, with only one free parameter, β. This preconditioning technique can also be applied to unsteady calculations using dual-time stepping algorithm. Any practical implementation of preconditioning should provide an ultimate net gain in terms of convergence acceleration, taking into account the additional computational cost of the preconditioning itself. The following outlines how the implementation is achieved.

Matrix P_0 is applied to characteristics variables $d\varpi=(dp/\rho c, du, dv, dw, dp-c^2d\rho)^T$. For conservative variables in most density-based flow solvers, the preconditioning matrix becomes:

$$P_c = \frac{\partial w}{\partial \bar{w}} P_0 \frac{\partial \bar{w}}{\partial w}$$

This form and the forms below involve too much matrix multiplication that needs to be reduced. The preconditioned dual-time stepping algorithm with Jameson's modified Runge-Kutta integration is as follows:

$$\begin{aligned} \mathbf{W}^{(0)} &= \mathbf{W}_H^l \\ \left(\mathbf{I} + \alpha_k \overline{\lambda} \mathbf{P}\right) \mathbf{W}^{(k)} &= \mathbf{W}^{(0)} + \alpha_k \overline{\lambda} \mathbf{P} \mathbf{W}^{(k-1)} - \alpha_k \mathbf{P}\, \mathcal{L}_{IRS}\left[\Delta t^* (\mathcal{R}^*(\mathbf{W}) + T_H)\right] \\ \mathbf{W}_H^{l+1} &= \mathbf{W}^{(m)}, \end{aligned}$$

where W is the conservative variable vector, $\overline{\lambda} = 3\Delta t^* / 2\Delta t$ for second-order backward Euler formulation. Δt* is the fictitious time step, and Δt the physical time step. T_H is the forcing term from multi-grid cycles, which appears only on coarse grid levels. The implicit residual smoothing (IRS) operator is an optional step.

Recognize the following matrix product with a vector $\vec{x}$,

$$(\mathbf{I} + \sigma\,\mathbf{P})^{-1}\vec{x} \;=\; \frac{1}{1+\sigma}\left(\vec{x} - \sigma\, z(\vec{x})\frac{\beta^2-1}{1+\sigma\,\beta^2}\frac{\gamma-1}{c^2}\,\vec{s}\right)$$

$$(\mathbf{I} + \sigma\,\mathbf{P})^{-1}\cdot\mathbf{P}\cdot\vec{x} = \frac{1}{1+\sigma}\left(\vec{x} + z(\vec{x})\frac{\beta^2-1}{1+\sigma\,\beta^2}\frac{\gamma-1}{c^2}\,\vec{s}\right)$$

where $\sigma = \alpha_k\overline{\lambda}$, $\vec{s} = (1, u, v, w, H)^T$, $z(\vec{x}) = \frac{q^2}{2}x_1 - ux_2 - vx_3 - wx_4 + x_5$, $q^2 = u^2 + v^2 + w^2$. The flow variable update can then be written as

$$\mathbf{W}^{(k)} \;=\; \underbrace{\frac{1}{1+\sigma}\left(\mathbf{W}^{(0)} + \sigma\,\mathbf{W}^{(k-1)} + \mathbf{R}\right)}_{\text{non-conditioned update}} + \underbrace{\left(\sigma\, b\, z(\mathbf{W}^{(k-1)} - \mathbf{W}^{(0)})\right)}_{\text{point-implicit term}}\vec{s} + b\, z(\mathbf{R})\,\vec{s}$$

where $\mathbf{R} = -\alpha_k\mathcal{L}_{IRS}[\Delta t^*(\mathcal{R}^*(\mathbf{W}) + T_H)]$ $\quad b = \dfrac{(\beta^2-1)(\gamma-1)}{(1+\sigma)(1+\sigma\,\beta^2)c^2}$

Notice that the first term on the right-hand side of the above equation is exactly the update of the non-conditioned Runge-Kutta stage. The second term is the result of point-implicit treatment, which is a function of the difference of the conservative variables. At the 1st stage of the Runge-Kutta scheme, this term is zero. At subsequent Runge-Kutta stages, however, this term reflects the difference between the latest availability of W and its starting value at each fictitious time step. Let

$$\tilde{\mathbf{W}}^{(k-1)} = \frac{1}{1+\sigma}\left(\mathbf{W}^{(0)} + \sigma\,\mathbf{W}^{(k-1)} + \mathbf{R}\right), \quad \text{and} \quad \mathbf{D} = \sigma\left(\mathbf{W}^{(k-1)} - \mathbf{W}^{(0)}\right) + \mathbf{R}.$$

We then have the final form for implementation

$$\mathbf{W}^{(k)} = \tilde{\mathbf{W}}^{(k-1)} + b\, z(\mathbf{D})\,\vec{s}.$$

It clearly indicates that the only addition to the existing dual-time stepping procedure is the second term of the above equation. This term consists of a coefficient and a simple vector, leaving no trace of matrix multiplication. The coefficient is a simple function of control parameter β, conservative variables, and residuals. This final form effectively reduces the overhead cost of the preconditioning approach to its bare minimum.

F. An Alternative Algorithm for Unsteady Flow Solutions

One significant factor that limits the Hi-Fi CFD to be performed routinely is that it takes a long time to obtain a converged solution. Besides the physical reasons of flow settling down in a large domain, and practical reasons that time accurate solutions need to be obtained, the numerical algorithm for unsteady flow is most to blame for the long solution time. The alternative algorithm described below follows the general dual-time approach but seeks to reduce the solution time by an order of magnitude. The dual-time stepping technology has proven to be an effective method and is widely used. With a simple point-implicit treatment, the algorithm is stable for all time steps. The long computational time comes from the fact that the inner iteration of the dual-time stepping has to be converged to an accepted level; and that each inner iteration is driven by the modified multi-stage Runge-Kutta scheme with usually 3 levels of multigrid. It is difficult to measure the time discretization error if the inner iteration is not fully converged. Practically, it's hard to determine how many inner iterations are sufficient for complex flows. On the other hand, if the unsteady Navier-Stokes equations are solved in a direct-time-marching fashion with ADI schemes, the ADI schemes can generally provide second-order accuracy. However, the ADI schemes introduce linearization error, factorization error, and extra computational costs for calculating and inverting Jacobian matrices. They are also conditionally stable in three-dimensional problems. This limits the free choice of the physical time step.

The alternative algorithm seeks to combine the advantages from both the implicit schemes (certainty of accuracy) and the explicit schemes (low cost). This algorithm is described as follows.

$$\frac{3}{2\Delta t}w^{n+1} - \frac{2}{\Delta t}w^{n} + \frac{1}{2\Delta t}w^{n-1} + R(w^{n+1}) = 0. \tag{1}$$

$$\left\{I + \frac{2\Delta t}{3}(D_xA + D_yB + D_zC)\right\}\Delta w^{n} + \frac{2\Delta t}{3}R(w^{n}) - \frac{1}{3}\Delta w^{n-1} + \mathcal{O}(\left\|\Delta w^{2}\right\|) = 0. \tag{2}$$

$$LD^{-1}U\Delta w^{n} + \frac{2\Delta t}{3}R(w^{n}) - \frac{1}{3}\Delta w^{n-1} + \mathcal{O}(\left\|\Delta w^{2}\right\|) + \mathcal{O}(\Delta t^{2}) = 0. \tag{3}$$

$$\begin{aligned} LD^{-1}U\Delta w^{k} &\underbrace{-LD^{-1}U\Delta w^{k-1} + \left\{I + \frac{2\Delta t}{3}(D_xA + D_yB + D_zC)\right\}\Delta w^{k-1}}_{\text{factorization error}} \\ &+ \frac{2\Delta t}{3}R(w^{n}) - \frac{1}{3}\Delta w^{n-1} + \mathcal{O}(\left\|\Delta w^{2}\right\|) = 0; \end{aligned} \tag{4}$$

or

$$\begin{aligned} &LD^{-1}U(\Delta w^{k} - \Delta w^{k-1}) \\ &+ \underbrace{\left\{I + \frac{2\Delta t}{3}(D_xA + D_yB + D_zC)\right\}\Delta w^{k-1} + \frac{2\Delta t}{3}R(w^{n}) - \frac{1}{3}\Delta w^{n-1}}_{\text{linearized total residual}} + \mathcal{O}(\left\|\Delta w^{2}\right\|) = 0. \end{aligned} \tag{5}$$

$$LD^{-1}U(\Delta w^{k} - \Delta w^{k-1}) + \underbrace{\frac{3}{2\Delta t}w^{k-1} - \frac{2}{\Delta t}w^{n} + \frac{1}{2\Delta t}w^{n-1} + R(w^{k-1})}_{\text{nonlinear total residual}} = 0, \tag{6}$$

where

$$\Delta w^{0} = 0.$$

The full implicit backward Euler (second order in time) of the Navier-Stokes equations is written in Eq.(1), where w is the conservative variable vector, R the residual, and Δt the physical time step. Eq.(1) is then linearized and recast in the delta-form in Eq.(2). The linearization error is introduced in Eq.(2). Eq.(3) is resulted when the LU factorization is introduced to Eq.(2). This form is the conventional implicit direct-solve (non-dual-time stepping) algorithm, which bears a nominal second-order accuracy. Now, consider forming an iterative process to solve Eq.(3) by compensating the factorization error obtained from the previous iteration, we then have Eq.(4). Upon convergence of this iterative process the factorization error will be fully compensated. Recasting Eq.(4) leads to Eq.(5), where the terms of interest are underlined. This group of terms is recognized as the linearized total residual (see Eq.(2)), which includes the second-order accurate time derivative term and the flux balance (R(w)). There is no need to solve Eq.(5) as is, because we can replace the linearized total residual with the original nonlinear residual. This is expressed in Eq.(6). The LU operation is performed on the difference of the difference of the conservative vector. If we take the LU decomposition approach given by Yoon and Jameson[12], we do not need to perform matrix inversion. In addition, if we follow the LU solution procedure proposed by Jameson and Caughey[13], we do not need to perform any matrix operation when evaluating the flux balances. This limits the total cost of the solution procedure of Eq.(6) to that of a four-stage Runge-Kutta scheme. Other benefit includes that no additional memory allocation is needed which is otherwise typical for implicit algorithms. This fast alternative to the traditional dual-time stepping algorithm is expected to reduce the number of inner iterations (of dual-time stepping) to just a few, which is typically an order of magnitude reduction comparing to the dual-time stepping algorithm.

IV. Interrogation and Interpretation of Unsteady Flows

Being able to simulate the unsteady flow, however accurate and fast, does not automatically imply that we understand the flow physics. Probing and understanding flow physics often require a different mindset; and the availability of unsteady flow CFD results gives the flow analysts both the freedom to explore and the challenge to sift through vast amount of information. This section summarizes what the authors have learned in the past few years on large-scale unsteady flow simulations and the way to probe and interrogate the numerical results.

A. Flow Physics

Flows going through the blades and vanes in turbine engines are inherently unsteady. Each blade generates a wake, which is convected downstream and ingested by downstream blade rows. As the wakes migrate, they are mixed out gradually. Shock waves are another significant source of unsteadiness in transonic compressors and fully

loaded turbines. Besides shock-boundary layer interaction, the impingement and reflection of shock waves directly affect the loading of adjacent blade rows. Vortices (hub/tip leakage flow, passage vortices, hub/tip vortices, etc) are secondary flows within blade passages and in between blade rows. Secondary flows cause aerodynamic losses, heat transfer problems, and mechanical issues. Besides the above-mentioned unsteadiness, there are also low frequency disturbances within aircraft engines, such as inlet and exit flow distortion and engine stall/surge. These low frequency modes often interact with the high frequency modes in a highly non-linear fashion. The advancement of numerical simulation in the last 15 years or so closely reflects the drive to understand the increasingly complex flow. Figure 3 illustrates the evolution of numerical simulation, going from single passage "steady-state" model to blade-row interactions, to component simulations, and to multi-disciplinary component interaction.

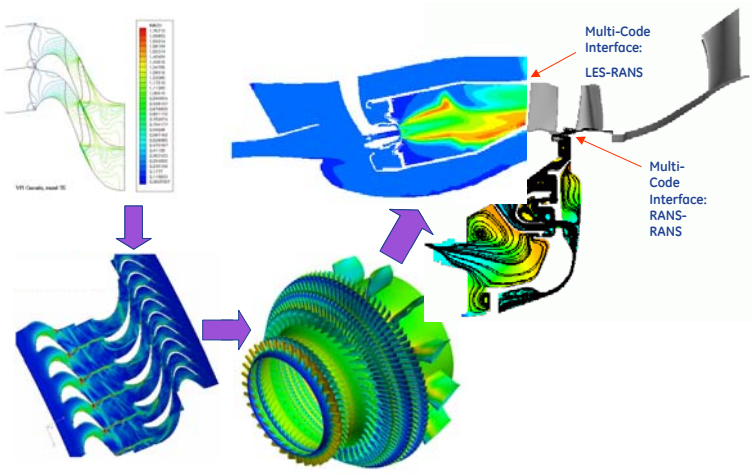

Figure 3. Increasing of modeling scope and fidelity since 1990's

The major difference between the unsteady flow and the steady-state flow is expressed in the following differential forms, by the first and second law of thermodynamics:

$$\frac{dh_0}{dt} = \frac{1}{\rho}\frac{\partial p}{\partial t}; \quad \text{and} \quad T_0 ds = dh_0 - \frac{1}{\rho_0} dp_0$$

1st law 2nd law

The time rate of change of pressure highlights the nature of unsteady flows. Whenever static pressure is changing in time, the total enthalpy (or total temperature) is also changing, which differentiates the unsteady flow from the "steady-state" assumption in that the total pressure of a given fluid particle may not in general remain constant, even if the flow is isentropic. Moreover, by the second law of thermodynamics, the change in total temperature may generate a commensurate change in total pressure without affecting thermodynamic loss. It is always useful to start with the static pressure change in time when investigating unsteady flows.

B. Loss Audit

Understanding losses in turbomachinery is an essential step in improving design for better performance. Loss sources in turbomachinery are perhaps the most-studied aspect, and it has been dissected into great detail. While these studies are fundamental and useful, one cannot afford to lose sight of the overall loss assessment. When unsteady flows are involved, assessing the loss due to unsteadiness is often demanded since the design process is still based on steady-state assumptions. By re-arranging the Navier-Stokes equations, the loss transport equation can be obtained in the form of entropy as follows:

$$\dot{s}_{\text{vol}} \equiv \rho \frac{Ds}{Dt} + \frac{\partial}{\partial x_i}\left(\frac{q_i}{T}\right) = \frac{1}{T}\tau_{ij}\frac{\partial u_i}{\partial x_j} + \frac{\kappa}{T^2}\left(\frac{\partial T}{\partial x_i}\frac{\partial T}{\partial x_i}\right)$$

Turb. Prod. Viscous Heat Transfer

Unlike turbulence, loss cannot be dissipated or diffused. It can only be convected and/or generated. The equation above gives a good illustration. The two terms of the right-hand side of the equation above are the sources of loss generation, which is often referred as entropy generate rate. The first term is related to turbulence production term, which is often found in turbulence transport equation of TKE (turbulence kinetic energy). The second term accounts for the viscous heat transfer loss. Both terms are denominated by temperature which explains why re-heat in power-generation turbomachinery works to improve efficiency.

Numerical simulations provide details of the flow field, upon which the loss production terms can be calculated. This information can then be assessed either locally, or can be integrated over selected regions such as hub or tip regions of a certain blade row. Take for instance the first term of the loss production; it is proportional to velocity gradient, assuming one-dimensional flow for simplicity of discussion.

$$\frac{1}{T}\tau_{ij}\frac{\partial u_i}{\partial x_j} \Rightarrow \left(\frac{\partial u}{\partial x}\right)^2$$

$$\overline{\left(\frac{\partial u}{\partial x}\right)^2} = \left(\frac{\partial \bar{u}}{\partial x}\right)^2 + \overline{\left(\frac{\partial u'}{\partial x}\right)^2}$$

(I) (II)

Term (I) is the loss based on time-averaged flow variables, which could be different from the loss calculated from "steady-state" simulations. But term (II) is directly associated with the unsteady flow (assuming u=ū+u', where u' is deterministic fluctuation). In three-dimensional flows, this term can be calculated as the difference of time-averaged loss (s_{vol}) and the loss that is calculated using the time-averaged flow variables.

An example of loss audit in facilitating design was reported by the authors in Ref. 14. In that investigation of HP turbine and LP turbine interaction loss, entropy generation reveals that additional loss is at shock/wake crossings, see Figure 4. Subsequent theoretical analysis of wake/shock interaction had indicated that the wake/shock interaction loss is proportional to shock strength and intersection angle. This interaction has also affected the turbulence level and flow capacity into the LP turbines. Redesign of the HP turbine blade had reduced the tail shock strength. As a result of shock strength reduction, the shock became more oblique, which reduced wake/shock interaction loss on two accounts. This led to a 0.4 point group efficiency gain for the LP turbine. The shock/wake interaction can also be found in fan and compressors in between stator vanes and downstream transonic rotor[1,2,3,15].

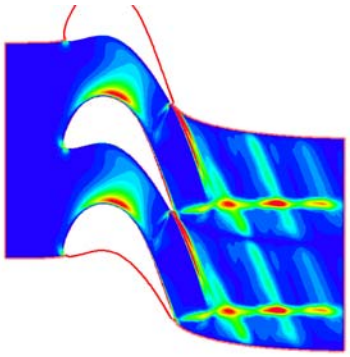

Figure 4. Entropy generation rate reveals shock/wake interaction loss

Entropy generation can be related to isentropic efficiency via the h-s diagram for both turbines and compressors. Illustrated in Figure 5 is the diagrams and efficiency definitions, assuming no external heat transfer and that the temperature remains constant along the line 2-2s. The loss of efficiency of a compressor is directly proportional to the increase in specific entropy through the machine and also to its exit temperature. The same is closely true for a turbine provided that the efficiency is high.

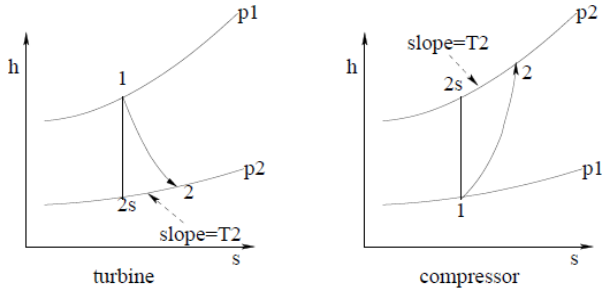

$$\eta_{\text{turbine}} = \frac{h_1 - h_2}{h_1 - h_2 + T_2(s_2 - s_1)},$$

$$\eta_{\text{compressor}} = \frac{h_2 - h_1 - T_2(s_2 - s_1)}{h_2 - h_1}.$$

Figure 5. Link between entropy generation and isentropic efficiency

C. Distortion Transfer in a Multi-Stage Fan System

Inlet flow distortion is a non-uniform total pressure, temperature, or swirl condition at the engine inlet. It can be radial, circumferential, or combined; steady or transient. Inlet distortion causes loss in engine stall margin and performance, and can also cause aeromechanics or noise issues. It is traditionally studied via expensive engine test often after the design is finalized. Extensive data correlation is used to guide engine design, trading performance with operability carefully. Recent advance on low-observance inlet technology poses a new challenge to engine design, since it produces complex distortion patterns that conventional distortion screens do not simulate. The need for physics-based, designed-in methodology for distortion handling is industry-wide.

A fan transfers some fraction of pressure distortion to the downstream compressor; it also generates temperature distortion, which is ingested by the compressor as well. Distortion handling is a major aircraft integration issue, as it

impacts many design decisions. During the past few years, the authors have applied Hi-Fi CFD trying to simulate and understand inlet flow distortion transfer and fan response in multistage fan systems [4, 5, 16, 17].

Two three-stage fans were selected for the numerical simulation. The two fans were subject to 20% and 35% (peak-to-peak) of one-per-rev total pressure distortion at inlet, respectively. The two fans and the boundary conditions are shown in Figure 6. The distortion transfer characteristics of the two fans are similar even though they were designed with different overall pressure ratio, wheel speed, and stage loading distributions. The results of the first fan will be used to illustrate the findings of this numerical analysis. The distortions of total pressure, total temperature at 50% span are shown in Figure 7 (left and middle columns). Total pressure distortion is the only distortion that the fan was subject to, but as a result of fan response, a total temperature distortion and a swirl distortion were also generated. See the left column in Figure 8 for swirl distortion generation.

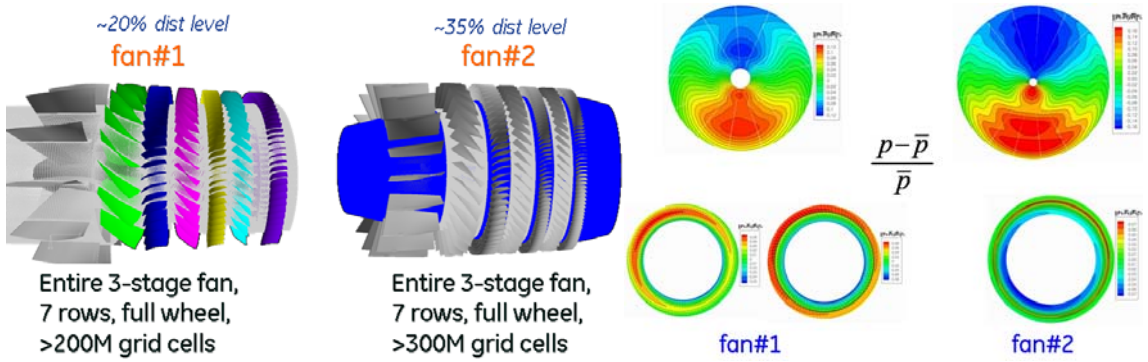

Figure 6. Computational domain and boundary conditions for distortion transfer

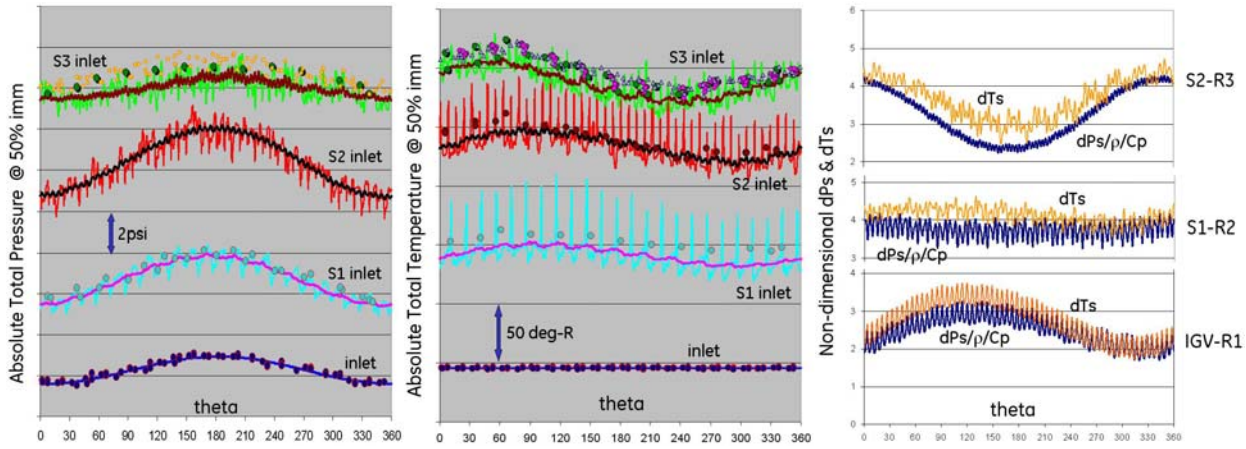

Figure 7. Distorted PTA and TT profiles at 50% span throughout a 3-stage fan

The numerical simulation did capture what the experimental measurement had revealed, which validated the overall CFD capability. Both CFD and data had indicated total temperature distortion generation and transfer. One investigation had focused on why the total temperature profile had a 90-degree "phase shift" with regard to the total pressure profile, and what caused another phase shift across the last stage in the total temperature profiles. We found that the static pressure and static temperature profiles follow their respective stagnation quantities closely. Further interrogation had traced to a relation among entropy, enthalpy, and pressure, also known as Gibb's equation.

$$Tds = CpdT - dp/\rho$$

The two terms of the above equation are shown in the right column of Figure 7, which clearly reveals how the total temperature profile formed across the first stage, and how the total temperature profile across the third stage changed in response to the pressure rise across that stage. This plot also reveals that aerodynamic loss within each stage is not a constant in the fan circumference; and that fan response of each of the three stages is quite different.

Swirl distortion within the fans was also analyzed and is shown in Figure 8 (left column). The first swirl distortion appeared before the flow reaches the IGV (inlet guide vane) though the swirl at inlet was uniform. This is due to the presence of static pressure distortion that is sustained by the fan. This induced swirl distortion was largely attenuated by the IGV. There are also swirl distortions within the blade row region, and this is a result of the fan responding to the pressure and temperature distortions. Flow features were also investigated. Figure 8 shows the shock structure of static pressure at design point and near stall point. At design point, a dual-shock structure appeared at high inlet Pt section, while a single shock was formed at low inlet PT sector. This indicated that rotor-3 was effectively "throttled" by the distortion even though the overall throttle of the fan remained constant. This reveals how the stability margin of the rotor is consumed by the distortion, in which the last stage might become a limiting stage for the overall stability of the fan.

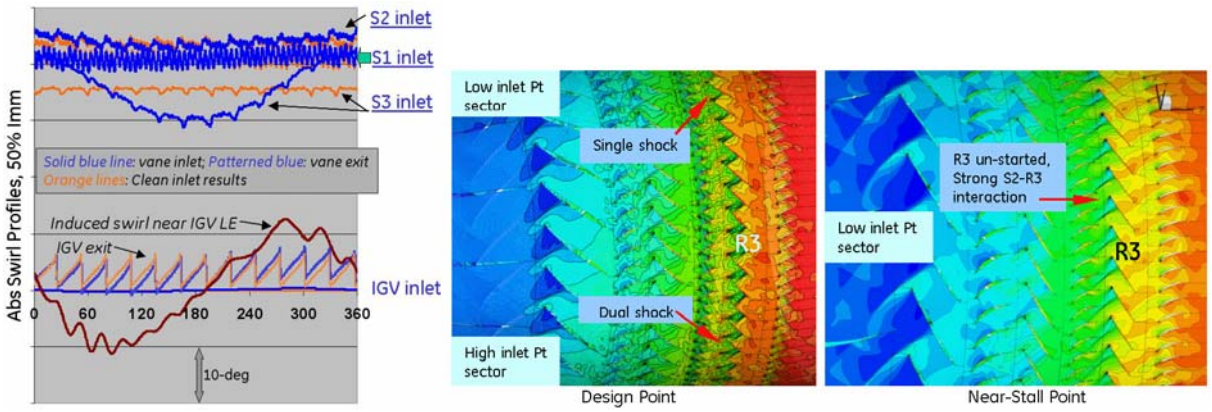

Figure 8. Swirl profiles (left) and Shock structures (right)

D. Distortion Analysis in a Commercial Fan System

A numerical analysis was also carried out on a commercial fan system, which includes the nacelle, the fan blade, the by-pass and core streams, the OGV, pylon, and strut. The fan rotor is subject to circumferential pressure and swirl distortions at inlet due to the nacelle (total pressure and total temperature are uniform); it is also subject to an exit pressure distortion set by the pylon and strut. The entire domain included full annuli of the above-mentioned components, resulting in a total of 170-million grid points. See Figure 9 for the entire computational domain. Subsets of the entire domain were also simulated for the purposes of isolating and quantifying the effects of different sources of distortion.

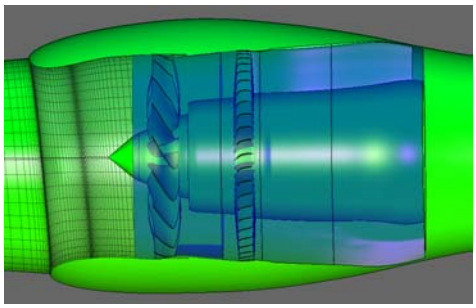

Figure 9. Integrated nacelle + fan + ogv + pylon + strut domain

Figure 10 is a series of pressure and swirl contour plots taken at the fan face. Pressure is normalized as $(p-p_{ave})/(p_{max}-p_{min})$, where p_{ave}, p_{max}, and p_{min} are the face average, maximum, and minimum. Results from three different simulations are plotted. The left column of the contour plot is steady-state nacelle solution, middle column is time-averaged nacelle/fan unsteady solution, and the right column is the time-averaged solution of the entire domain. It is clear that the fan/nacelle interaction has resulted in a different pressure pattern at the exit of the nacelle. The fan does not passively take the distortion generated by the nacelle; it plays an active role to modify the distortion as well. The high-low axis of pressure at outer diameter is "rotated" counter clockwise; while at the inner diameter, this "rotation" is more pronounced. The swirl distortion pattern, in response to the pressure pattern change, has also changed. The addition of OGV/pylon only changes the distortion pattern subtly but visibly. Integrating the inlet, fan, OGV and nozzle together in a mutual flow simulation offered the opportunity to better understanding how the distortion interacts with the various components, which can be used by the air-framers and engine manufacturers to further optimize the designs.

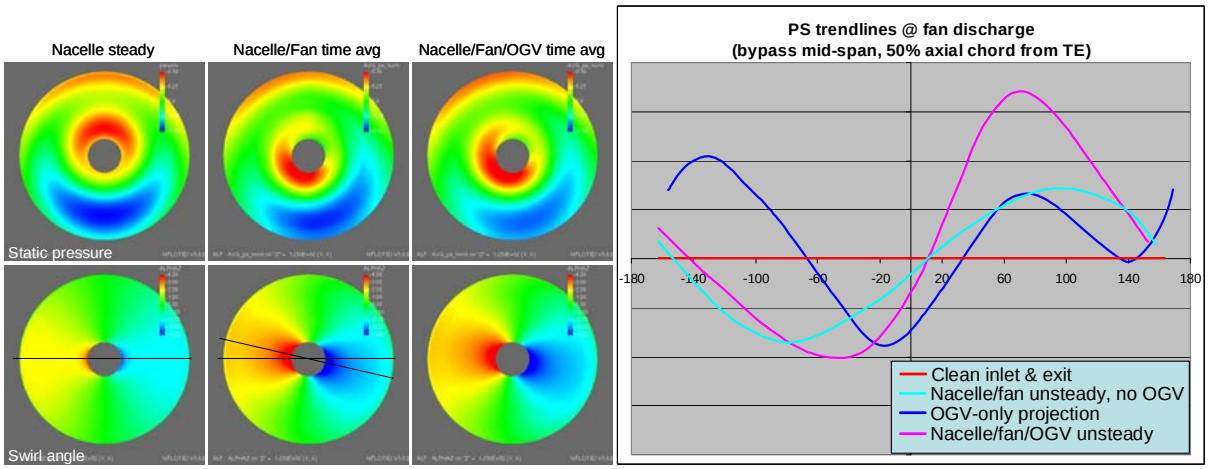

Figure 10. Pressure and swirl contours illustrating nacelle/fan interaction (left); Fan discharge pressure profiles in fan circumference at by-pass mid-span under various conditions (right)

At fan discharge, the circumferential pressure profile is not expected to be uniform due to the presence of structural members (pylon and strut) and OGV. Figure 10 also includes a plot of fan discharge pressure profiles (circumferential trendlines are shown) at about 50% axial chord downstream of the fan at various domain/boundary conditions. The structural members and OGV projected a one-per-rev pressure distortion to the fan exit, depicted by the blue line. This is the pressure profile without any influence from upstream flow conditions. On the other hand, if the fan only takes the inlet distortion due to the nacelle without any downstream effect, the result is the pressure profile shown in cyan. The pressure profile of integrated simulation, shown in pink, is manifested by the fan negotiating with distortion sources at both inlet and discharge. It is not a simple linear interaction. The inlet distortion, which has gone through the fan, but modified by the fan, is then ingested by the OGV. The OGV is thus affected by the distortion.

E. Unsteady Flow Solution and Deterministic Stress

The appearance of the so-called "deterministic" stresses in the time averaged RANS is a direct result of applying a time averaging process to the unsteady RANS equations. The unsteadiness of flows in turbomachinery obviously has the contributions of turbulence fluctuation, however, there exist other variations of flow in time that are not turbulence in nature, such as rotor/stator interaction, migration of all kinds of vortices in hub/tip gaps, migration of hot streaks, etc. In normal operating conditions, the unsteadiness of the flow in turbomachinery comes mainly from the relative motion of blade rows. The rotor revolution also forms the periodicity of the unsteadiness. Hence, the rotating period of a rotor is the common time scale in the unsteady flow field. This time scale is at least several orders of magnitude larger than the turbulence fluctuation period. This draws a distinct line between turbulence and the deterministic unsteadiness, and makes it valid to assume that the mean and the fluctuation components are not correlated; hence the time average of their product diminishes.

$$\begin{bmatrix} \overline{\rho u_r'' u_r''} & \overline{\rho u_r'' u_\theta''} & \overline{\rho u_r'' u_z''} \\ \overline{\rho u_\theta'' u_r''} & \overline{\rho u_\theta'' u_\theta''} & \overline{\rho u_\theta'' u_z''} \\ \overline{\rho u_z'' u_r''} & \overline{\rho u_z'' u_\theta''} & \overline{\rho u_z'' u_z''} \\ \overline{\rho u_r'' H''} & \overline{\rho u_\theta'' H''} & \overline{\rho u_z'' H''} \end{bmatrix}$$

$$\overline{\rho u'' v''} = \overline{\rho u v} - \overline{\rho u}\,\overline{\rho v}/\overline{\rho}$$

Figure 11. Deterministic stress terms and their evaluation

The "time-averaging" manipulation is strictly mathematical in nature, and introduces no additional physical principles. At no point will this procedure balance our unknowns/equation ledger. However, the deterministic stress terms do provide a detailed measure of flow unsteadiness in nine (9) major correlation terms if we ignore turbulence-related terms, shown in Figure 11. Six of the nine terms are related to velocity-velocity product, and three of them are velocity-enthalpy product, derived from the energy equation. We chose not to elaborate on the difficulties of modeling of the stress terms due to limitation of the scope of this paper. But we will need to examine how to interpret loss due to the addition of these terms to the "steady-state" RANS equations. Below is an analysis using small perturbation to the 3-D Euler equation with deterministic source terms:

$$\begin{cases} \dfrac{\Delta(\rho u_j)}{\Delta x_j} = 0 \\ \dfrac{\Delta(\rho u_i u_j + p\delta_{ij})}{\Delta x_j} + D_m = 0 \\ \dfrac{\Delta(\rho u_j H)}{\Delta x_j} + D_e = 0 \end{cases} \qquad \Delta s = \frac{R}{\gamma - 1}\frac{\Delta p}{p} - Cp\frac{\Delta \rho}{\rho} = \frac{R}{p}\left(D_m - \frac{D_e}{\overline{u}_i} \right)\Delta x_j$$

$$= \frac{R}{p}\left(\frac{\partial \overline{\rho u_i' u_j'}}{\partial x_j} + \frac{\partial \overline{\rho H' u_j'}}{\overline{u}_i \partial x_j} \right)\Delta x_j$$

Consider $\overline{\rho H' u_j'} = Cp\,\overline{\rho u_j' T} + \overline{u}_i\,\overline{\rho u_i' u_j'} + \tfrac{1}{2}\,\overline{\rho u_j' u_i' u_i'}$

We have $$\Delta s = -\frac{R}{p\,\overline{u}_i}\left(Cp\,\frac{\partial\,\overline{\rho u_j' T}}{\partial x_j} + \overline{\rho u_i' u_j'}\,\frac{\partial \overline{u}_i}{\partial x_j} + \frac{1}{2}\frac{\partial\,\overline{\rho u_j' u_i' u_i'}}{\partial x_j} \right)\Delta x_j$$

The entropy change is determined by the balance of source terms from the momentum equation and from the energy equation. The entropy change can be interpreted in two ways: (a) locally at a control volume, the entropy is increased or decreased based on the balance of local *gradient* of the deterministic stresses; (b) globally between the "steady" state and the "time-averaged" flow state. This balance, either locally or globally, does not always come out as entropy increase. Negative entropy increase means energy is added to the system by the deterministic terms. Examples include fan leading edge shock input to the nacelle, or HP turbine trailing edge shock migrating into inter-turbine space and LP turbine region.

V. Challenges and Outlook of Hi-Fi Numerical Simulations

A. Faster and Versatile Flow Solver

As a building block, the basic CFD capability on RANS level needs further improvement to be able to predict wider range of flows. Better resolving tip leakage flows, transitional flows, and rotating stall requires significant improvement of turbulence modeling and robust algorithms. For unsteady flows, time-to-solution is still a prohibiting factor for quick turn-around. This is at odds with the numerical scheme improvement, as that tends to increase computational cost. Most current industrial CFD codes were developed and validated before massively parallel computing was available. These codes are parallelized to adapt to the HPC environment while still carrying a lot of legacy data and control structures. Re-writing these codes for petascale computers may seem to be an additional cost, but if the resultant codes are significantly faster than the old ones, it is certainly worth pursuing. One way to achieve high parallel efficiency and scalability for structured mesh with domain decomposition is to separate the highly parallelizable core from the pre-processing, initialization, and post-processing that were built within the existing codes over time.

The versatility of CFD solvers is also required to effectively deal with turbomachinery blade-row type geometry and non-blade row type geometry, such as engine nacelle, external flows upstream and downstream of the engine. Assumptions based on cylindrical coordinate system may need to yield to Cartesian based coordinate system. This is also a basic requirement as CFD is seeing more inter-disciplinary applications in the industry. Examples include aero and thermal coupling in turbine blades and vanes, aero and aeromechanics coupling for fan and compressor blades, and even combustor-turbine coupling.

B. Reduced-Order Modeling

The flow solver advancement discussed above is just means for us to complete solution and comprehend solution faster; the ultimate challenge is how to close the loop with the design processes. This is a critical step, as the value of CFD is only realized through this step for better performing engines. This bridge between the unsteady CFD and design is not just an understanding of the flow physics, but also a design space exploration using the newly acquired information and/or design freedom. If the understanding of flow physics can turn into an effective model at reduced order of fidelity, the design space exploration would then follow. For the inlet flow distortion transfer and generation, the authors have been experimenting with various models with reasonable success, and will report the outcome of the research in the near future. However, a great challenge still remains as how to management inlet distortion with robust and fail-safe means. And an ever-greater one is how to design engines with distortion tolerance.

C. Design for Unsteady Flows

Inevitably we need to incorporate the time dimension in engine design to achieve a higher time-mean performance. We can start this by growing the current design practice from a single blade row with steady-state assumption to a stage where the rotor and stator interact with each other. One possible approach is to optimize the spatial relationship of the two adjacent edges (trailing edge of upstream row and leading edge of downstream row), as they are the main initiators for blade row interaction. The spatial 3D profiles of the two edges represent the radial timing distribution of the interaction, and optimization could lead to much less variation in integrated quantities such as mass flow, torque, aero-mechanical forces. Design for unsteady flow is still in conceptual stage for now; realizing it will bring another significant improvement to aircraft engines in both performance and operability.

VI. Conclusions

Ever since Tournaire[18] presented the concept of multistage turbines and compressors in 1853, turbomachinery has never stopped improving in all aspects. We have accumulated a great wealth of the insight into the unsteady flow physics in turbomachines via theoretical analyses, experimental measurements, and recently numerical simulations. In today's engine design process, three-dimensional, steady-state flow analysis is an integrated element. The simulation of unsteady flows still, in many cases, remains as an elaborate tool for post-design analysis. It could continue to be that way, or it could be incorporated into the design process or early design phases just like the full 3D steady-state flow analysis replaced quasi-3D stream-surface approach. It is not the lack of information toward the unsteady flows for the latter to happen, it is rather the lack of commitment to transformation for the incorporation of the time dimension to happen. Only under the driving forces of commitment can the techniques of unsteady flow simulation and analysis be matured, yielding perhaps the last significant improvement of engine aero-performance.

Unsteady flow simulations have grown from blade-row interaction, to component interaction, and further to inter-disciplinary analysis. This requires us to broaden our knowledge domain on multiple disciplines, and to work the numerical simulations concurrently with advances of experimental measurements and high-performance computing. The aspects of unsteady flow simulation and analysis discussed in the paper are limited and are only based on our experience to date. With great details and immense amount of information produced by the Hi-Fi simulations, it could be detrimental for us to understand the underlying mechanisms, as greater details tend to conceal rather than reveal reality. This is often an over-looked challenge. Seeing both the big picture and the great details are often not adequate, we need to probe the "dynamic interplay" of flow phenomena under various conditions. This in turn requires analytical minds that can "zoom" in and out of the flow to discover cause-and-effect or correlations.

Acknowledgments

The authors would acknowledge the following individuals at GE Aviation, GE Global Research, and the US Air Force Research Labs: Peter Szucs, Peter Wood, Tom DiBiase, Scott McNulty, Andy Breeze-Stringfellow, Steve Putterbaugh, Mike List for numerous and insightful communications on topics covered in this paper. The authors would like to thank the DoD High Performance Computing Modernization Program Office and the Aeronautical System Center Major Shared Resource Center for the Challenge Award that provided the high performance computing resources. The authors would also like to thank the Advanced Virtual Engine Test Cell (AVETeC), Inc for the funding support in 2007 and 2008. The authors also appreciate that the paper is allowed to publish.

References

[1]Gorrell, S. E., Car, D., Puterbaugh, S. L., Estevadeordal, J., and Okiishi, T. H., 2006, "An Investigation of Wake-Shock Interactions With Digital Particle Image Velocimetry and Time-Accurate Computational Fluid Dynamics," *ASME J. Turbomachinery*, 128, pp. 616–626.

[2]Langford, M. D., Breeze-Stringfellow, A., Guillot, S. A., Solomon, W., Ng, W. F., and Estevadeordal, J., 2007, "Experimental Investigation of the Effects of a Moving Shock Wave on Compressor Stator Flow," *ASME J. Turbomachinery*, 129, pp. 127–135.

[3]van de Wall, A., Breeze-Stringfellow, A., and Dailey, L., 2006, "Computational Investigation of Unsteady Flow Mechanisms in Compressors With Embedded Supersonic Rotors," ASME Paper No. GT-2006-90633.

[4]Yao, J., Gorrell, S. E., Wadia, A. R. "High-Fidelity Numerical Analysis of Per-Rev-Type Inlet Distortion Transfer in Multistage Fans - Part I: Simulations with Selected Blade Rows", ASME Turbo Expo 2008: Power for Land, Sea and Air, June 2008, Berlin, Germany, GT2008-50812, to published on ASME J. of Turbomachinery

[5]Yao, J., Gorrell, S. E., Wadia, A. R. "High-Fidelity Numerical Analysis of Per-Rev-Type Inlet Distortion Transfer in Multistage Fans - Part II: Entire Component Simulation and Investigation", ASME Turbo Expo 2008: Power for Land, Sea and Air, June 2008, Berlin, Germany, GT2008-50813, to be published on ASME J. of Turbomachinery
[6]Turner, M. G., Gorrell, S. E., and Car, D., 2005, "Radial Migration of Shed Vortices in a Transonic Rotor Following a Wake Generator: A Comparison Between Time Accurate and Average Passage Approach," ASME Paper No. GT2005-68776.
[7]Dongarra, J. "Four Important Concepts that Will Effect Math Software", 9th International Workshop on State-of-the-Art in Scientific and Parallel Computing, May 13-16, NTNU, Trondheim, Norway
[8]Yao, J. "Development and Validation of a Massively Parallel Flow Solver for Turbomachinery Flows", *AIAA Journal of Propulsion and Power*, Vol. 17, No. 3, 2001, pp659-668
[9]Mortensen, C. H., Woodley, R. S., and Gorrell, S. E., "Concurrent Agent-enabled Extraction of Computational Fluid Dynamics (CFD) Features in Simulation", *Proceedings of The 2009 International Conference on Data Mining*, pp. 90 – 96, July, 2009.
[10]Mortensen, C. H., Gorrell, S. E., and Woodley, R. S., "An Intelligent Agent Architecture for Concurrent CFD Feature Extraction", AIAA Paper 2010-1323, January, 2010.
[11]E. Turkel and V. N. Vatsa. "Choice of variables and preconditioning for time dependent problems", AIAA Paper 2003-3692 CP, 2003.
[12]Yoon, S., Jameson, A. "A Multigrid LU-SSOR Scheme for Approximate Newton Iteration Applied to the Euler Equation", NASA CR 179524, Sept. 1986
[13]Jameson, A., Caughey, D. A., "How Many Steps are Required to Solve the Euler Equations of Steady Compressible Flow: In Search of a Fast Solution Algorithm", AIAA Paper 2001-2673, 15th AIAA Computational Fluid Dynamics Conference, June 11-14, 2001, Anaheim, CA.
[14]Yao, J. Carson, S. "HPT/LPT Interaction and Flow Management in the Inter-Turbine Space of a Modern Axial Flow Turbine", ASME Turbo Expo 2008: Power for Land, Sea and Air 2006, May, Barcelona, Spain, GT2006-90636
[15] List, M. G., Gorrell, S. E., Turner, M. G., "Investigation of Loss Generation in an Embedded Transonic Fan Stage at Several Gaps Using High Fidelity, Time-Accurate CFD," *ASME Journal of Turbomachinery*, Vol. 132, 011014, January 2010.
[16]Yao, J., Gorrell, S. E., Wadia, A. R. "A Time-Accurate CFD Analysis of Inlet Distortion Induced Swirl in Multistage Fans", 43rd AIAA/ASME/SAE/ASEE Joint Propulsion Conference & Exhibit, AIAA Paper 2007-5059, to be published on AIAA J. of Propulsion and Power
[17]Gorrell, S. E., Yao, J., and Wadia, A. R., "High Fidelity URANS Analysis of Swirl Generation and Fan Response to Inlet Distortion," AIAA Paper 2008-4985, July, 2008.
[18]Suplee, H. H. "The Gas Turbine", J. B. Lippincott Company, 1910 (digital copy by google.com)